Local structure and site occupancy of Cd and Hg substitutions in CeTIn$_5$ (T=Co, Rh, and Ir)

C. H. Booth,[1] E. D. Bauer,[2] A. D. Bianchi,[3,4] F. Ronning,[2] J. D. Thompson,[2] J. L. Sarrao,[2] Jung Young Cho,[5] Julia Y. Chan,[5] C. Capan,[3] and Z. Fisk[3]

[1]*Chemical Sciences Division, Lawrence Berkeley National Laboratory, Berkeley, California 94720, USA*

[2]*Materials Physics and Applications Division, Los Alamos National Laboratory, Los Alamos, New Mexico 87545, USA*

[3]*Department of Physics, University of California, Irvine, California 92697, USA*

[4]*Département de Physique et RQMP, Université de Montréal, Montréal, QC, H3C 3J7, Canada*

[5]*Department of Chemistry, Louisiana State University, Baton Rouge, Louisiana 70803-1804, USA*

(Received 5 February 2009; published 22 April 2009)

The CeTIn$_5$ superconductors (T=Co, Rh, or Ir) have generated great interest due to their relatively high-transition temperatures, non-Fermi liquid behavior, and their proximity to antiferromagnetic order and quantum critical points. In contrast to small changes with the T species, electron doping in CeT(In$_{1-x}M_x$)$_5$ with M=Sn and hole doping with Cd or Hg have a dramatic effect on the electronic properties at very low concentrations. The present work reports local structure measurements using the extended x-ray absorption fine-structure (EXAFS) technique that address the substituent atom distribution as a function of T, M, and x, in the vicinity of the superconducting phase. Together with previous measurements for M=Sn, the proportion of the M atom residing on the In(1) site, $f_{\mathrm{In}(1)}$, increases in the order M=Cd, Sn, and Hg, ranging from about 40% to 70%, showing a strong preference for each of these substituents to occupy the In(1) site (random occupation=20%). In addition, $f_{\mathrm{In}(1)}$ ranges from 70% to 100% for M=Hg in the order T=Co, Rh, and Ir. These fractions track the changes in the atomic radii of the various species, and help explain the sharp dependence of T_c on substituting into the In site. However, it is difficult to reconcile the small concentrations of M with the dramatic changes in the ground state in the hole-doped materials with only an impurity-scattering model. These results therefore indicate that while such substitutions have interesting local atomic structures with important electronic and magnetic consequences, other local changes in the electronic and magnetic structure are equally important in determining the bulk properties of these materials.

DOI: 10.1103/PhysRevB.79.144519 PACS number(s): 72.15.Qm, 61.05.cj, 71.23.−k, 71.27.+a

I. INTRODUCTION

The rich variety of novel strongly-correlated electron phenomena observed in the family of CeTIn$_5$ (T=Group VIII transition metal) heavy-fermion compounds,[1] such as the coexistence of unconventional superconductivity and magnetism under pressure[2,3] or through chemical substitution,[4,5] and magnetic field-induced magnetism within the superconducting state,[6–8] has invigorated interest in understanding the interplay of superconductivity and magnetism in strongly-correlated materials. The CeTIn$_5$ family (generically referred to as the "115s") is ideally suited to explore this interplay as the energy scales of these two ground states are easily tuned with modest pressures or magnetic fields. Recent work has focused on the effects of substitutions onto the In sites (Fig. 1), effectively either electron doping with Sn (Ref. 9) or hole doping with Cd (Ref. 10) or Hg.[11] Previous local structure studies of the atomic environment around the Sn atoms using the extended x-ray absorption fine-structure (EXAFS) technique found that Sn atoms preferentially reside on the In(1) site, helping explain the sharp dependence of the superconducting (SC) transition temperature, T_c, on the Sn concentration and further supporting the notion of quasi-two-dimensional superconductivity confined primarily to the Ce-In(1) planes.[12] Subsequent studies have shown that hole doping produces even more dramatic effects, including accessing the antiferromagnetic (AFM) phase and exhibiting reversible behavior under applied pressure.[10,11] It is therefore vital to determine the distribution of Cd and Hg on the In sites in these materials to properly assess the role that impurity scattering plays in the properties of the hole-doped 115 materials. The present study extends the previous study on CeCo(In$_{1-x}$Sn$_x$)$_5$ and determines these distributions using the EXAFS technique as a function of the species of M in CeCo(In$_{1-x}M_x$)$_5$ with M=Cd and Hg, and as a function of T in CeT(In$_{1-x}$Hg$_x$)$_5$ with T=Co, Rh, and Ir.

The substitution of Cd or Hg for In at the percent level in CeTIn$_5$ has revealed a simple way to continuously tune between SC and AFM order (Fig. 2) while introducing minimal structural disorder. In particular, T_c remains nearly constant with increasing Cd substitution up to x=0.5% from 2.3 K in pure CeCoIn$_5$. Superconductivity coexists with long-range AFM order for $0.5\% < x \leq 1.25\%$, after which point only AFM order is observed.[10] (Note that concentrations as measured by microprobe measurements of Cd and Hg are reported throughout this article, which are very close to 10% of the nominal concentration reported previously.[10]) The entropy balance between these ground states, along with the observation of coupled SC- and AFM-order parameters by neutron diffraction, implies that the same electronic degrees of freedom determine the nature of the ground state in these materials.[13] The application of pressure to CeCoIn$_5$:Cd reverses the evolution of the ground state with Cd substitution and also mimics the pressure-induced behavior of CeRhIn$_5$ (Ref. 3) in which AFM order is suppressed from its ambient pressure value of T_N=3.8 K to zero temperature by ~2.3 GPa, and coexists with superconductivity in an intermediate pressure range between 0.5 and 1.7 GPa. However, for the small Cd concentrations that induce these changes,

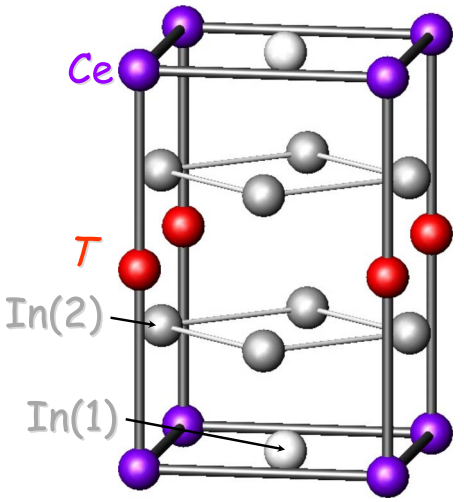

FIG. 1. (Color online) The tetragonal unit cell of the Ce-115s.

there is little detectable change in the average structure.[10] These results suggest that it is the slight hole-doping of $CeCoIn_5$ with Cd that tunes the electronic structure sufficiently to induce magnetism, rather than chemical pressure or disorder effects.

This behavior contrasts with that achieved by electron doping with Sn into Ce*T*In_5, which uniformly suppresses AFM order in $CeRhIn_5$ by 7% Sn for In without inducing superconductivity,[9] and completely suppresses superconductivity in $CeCoIn_5$ at 3–4% Sn with no sign of AFM order.[14,15] This behavior is more congruous with that achieved by substituting with La on the Ce site,[16] especially when considering the propensity of Sn to rest on the in-plane In(1) site.[12] Even so, the reduction in T_c with the Sn In(1)-site occupancy remains sharper compared to La substitutions, providing further evidence that slight changes in electronic structure dominate the underlying physics in the substituted Ce*T*In_5 materials. Although Abrikosov-Gorkov-type[12,17–19] pair breaking undoubtedly plays some role, exactly how such minute quantities of these particular substituent atoms are able to tip the delicate balance between the nearly degenerate SC and AFM ground states in Ce*T*In_5, where substitution on the transition-metal site requires of order 30% to induce similar changes, is an important yet poorly understood issue in the interplay between these two phenomena.

Here, the local structure around Cd and Hg in Ce*T*In_5 using the EXAFS technique is reported to determine how the local environment affects the ensuing magnetism and superconductivity. The EXAFS technique, while only having a range of about 6 Å, provides a particularly powerful way of determining the local atomic environment around the substituent atoms, because a specific core-electron x-ray absorption process is chosen. Therefore, even though very little Cd or Hg exist in these materials, only scattering paths involving Cd or Hg contribute to the EXAFS signal. The main structural difference for differentiating between the In(1) and In(2) sites is the nearest-neighbor In(2)-*T* distance at about 2.8 Å, since the nearest neighbors to the In(1) site are Ce and In(2) at about 3.3 Å. Other differences in the local structures around the In(1) and In(2) sites also help determine the fraction of the substituent atoms on the In sites. In addition, EXAFS is useful for determining distortions from the average crystal structure, which may also be important in determining the effects of substitutions onto the In sites.

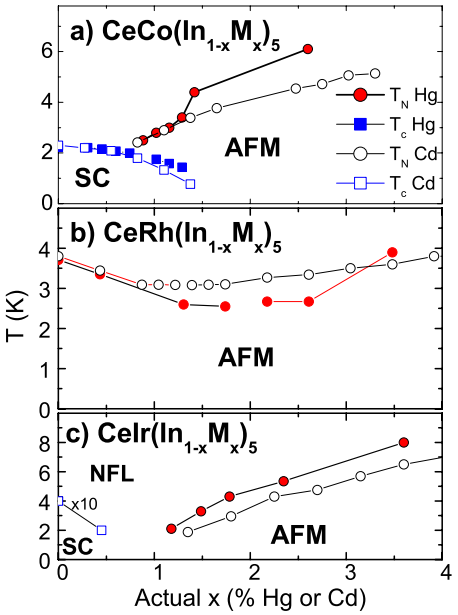

FIG. 2. (Color online) Phase diagrams of Cd- and Hg-substituted Ce*T*In_5. The reported substituent concentrations of some Cd-substituted samples are estimated from microprobe measurements of the Hg-substituted samples. See Sec. II for details.

The rest of this article is organized as follows: experimental methods and data fitting techniques are described in Sec. II, while the details of the results of the fits are in Sec. III. These results are related to various parameters in Sec. IV, such as T_c, the various atomic radii and the substituent In(1)-site occupancy. Finally, the main conclusions of this research are summarized in Sec. V.

II. EXPERIMENTAL METHODS

Samples were synthesized as described in Refs. 10 and 11. X-ray diffraction measurements on the Cd-substituted samples indicate contraction of both the *a*- and the *c*-lattice parameters of about 0.005 Å in the vicinity of the critical concentration x_c where the samples cease to be superconducting (Fig. 2). Measurements on the Sn- and Hg-substituted samples, however, have not been able to identify any clear trend in the lattice parameters with concentration. Microprobe analysis of $CeCo(In_{1-x}Cd_x)_5$ yielded an actual/nominal Cd concentration ratio $x_{act}/x_{nom}=0.11$, close to the value of 0.10 reported in Ref. 10. A similar analysis[20] yielded an actual/nominal Hg concentration ratio of 0.16, 0.17, and 0.18 for *T*=Co, Rh, and Ir, respectively. Lacking microprobe data for $CeRh(In_{1-x}Cd_x)_5$ and $CeIr(In_{1-x}Cd_x)_5$, the same actual/nominal Cd concentration ratio was used for a relative comparison to the Hg-doped $CeRhIn_5$ and $CeIrIn_5$ temperature-composition phase diagrams, given that Cd is isoelectronic with Hg.

The following samples were measured with the EXAFS technique for this study, although not all data are explicitly reported for the sake of brevity: $CeCo(In_{1-x}Cd_x)_5$ with $x=0.003$, 0.005, 0.011, and 0.18; $CeCo(In_{1-x}Hg_x)_5$ with $x=0.007$, 0.012, and 0.014; $CeRh(In_{1-x}Hg_x)_5$ with $x=0.009$, 0.026, and 0.035; and $CeIr(In_{1-x}Cd_x)_5$ with $x=0.009$, 0.018, and 0.036.

X-ray absorption data were collected at Beamline 11-2 of the Stanford Synchrotron Radiation Lightsource using half-tuned Si(220) monochromator crystals on the unfocused beam. The samples were prepared for these absorption measurements by grinding them in a mortar and pestle under acetone, with the resulting powder passed through a 32 μm sieve. This powder was brushed onto adhesive tape, which was then cut into strips and stacked, either in sufficient quantity to have reasonable fluorescence data from the Cd K and Hg L_{III} edges, or to obtain a change in the absorption across the In K edge of about 0.8 absorption lengths. The samples were placed in a liquid-helium flow cryostat at 30 K. Data at the Cd K or Hg L_{III} edges were collected in fluorescence mode and corrected for the dead time of the 32-element Ge detector.

Data reduction and fitting were performed using the RSXAP package[21,22] with scattering functions generated by the FEFF7 code.[23] In particular, data collected in transmission mode must be treated differently than data collected in fluorescence mode. For the In K-edge data collected in transmission mode, the absorption contribution from the desired core excitation, μ_a, was isolated from the total absorption by subtracting the contribution from other absorption processes, as determined from a fit to the pre-edge data and forcing the remaining absorption to follow a Victoreen formula.[24] The embedded atom absorption μ_0 was generated by fitting a 7-knot-cubic spline function through the data above the main absorption edge. The EXAFS function was then calculated using $\chi(k)=[\mu_a(k)-\mu_0(k)]/\mu_0(k)$, where $k=[2m_e(E-E_0)/\hbar^2]^{1/2}$, E is the incident photon energy, and E_0 is the photoelectron threshold energy as determined by the position of the half-height of the edge. Fluorescence data are treated similarly, but there are two important differences. First, the absorption processes from channels other than the desired excitation are already discriminated against by the energy-sensitive Ge detector, apart from much smaller corrections due to roughly constant background processes and Compton scattering of the direct beam into the energy window for the desired Cd K_α or Hg L_α fluorescence lines. For each absorption process, a fluorescence photon is generated, so overall changes in the fluorescence above the absorption edge already should include the overall decrease in the absorption described by the Victoreen formula. For these reasons, a different pre-edge background, μ_{pre}, is applied that only tries to isolate the desired fluorescence line. Second, self-absorption processes can play an important role, and are, in fact, the main factor in overall increases or decreases in the observed fluorescence.[25–27] A self-absorption correction[27] was applied, but was typically less than 2%. Examples of these data are shown in Fig. 3 as an illustration of the quality of the data. Note that all data were collected to 16.0 Å^{-1} except the Hg L_{III}-edge (12 284 eV) data for $CeIr(In_{1-x}Hg_x)_5$, which was limited to 11.5 Å^{-1} by the Ir L_{II} edge (12 824 eV).

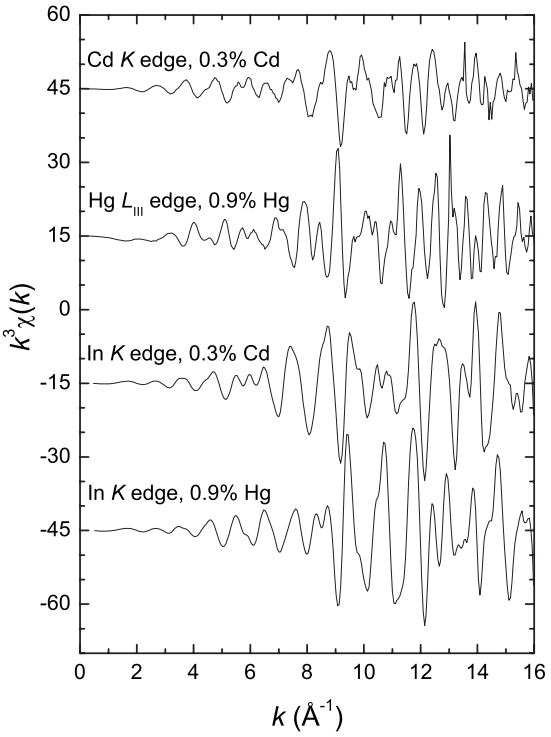

FIG. 3. Examples of k-space data at 30 K for representative samples of $CeCoIn_5$:Cd and $CeRhIn_5$:Hg at all three measured edges. These data are from averages of between three and six scans, each measured over about a half of an hour.

The 115 local structure around Ce and T-site atoms is relatively simple, with well separated scattering shells. The local structure around In is much more complicated, owing both to the two In sites and to strong overlap between In(1)-Ce, In(1)-In(2), In(2)-In(2), In(2)-In(1), and In(2)-Ce near neighbors, which are all near 3.3 Å. Although substituent atoms should appear in the backscattering [for instance, the In(1)-In(2) peak will overlap an In(1)-Hg(2) peak], such scattering shells have an insignificant contribution at the measured substituent concentrations. Such peaks are, in any case, included in the fitting model. In all, there are 20 single-scattering paths up to 5 Å. The bond lengths in the fitting model are therefore tightly constrained to the nominal 115 structure, equivalent to only allowing the variation of the a- and c-lattice parameters, the position z along the c axis of the In(2) sites, and, when the data allows, two additional atom-pair distances. Only the Cd-edge data and the Hg-edge data on the substituted $CeIrIn_5$ sample required tightening these constraints. In addition, many of the mean-squared displacements of the pair distances, σ^2's, are also constrained together. The number of neighbors per absorbing atom, N, are constrained to the nominal values, allowing both for an overall scale factor in the fit, S_0^2, the fraction of the absorbing atom on the In(1) site, $f_{In(1)}$, and the x value for the substituent concentration, only the latter of which is held fixed. Discrepancies between the actual structure and a fitting model of this type will manifest as enhanced values of the σ^2 parameters. Note that generally, only scattering paths with independent bond lengths in this model are reported in the tables for simplicity. The remaining independent parameters that are

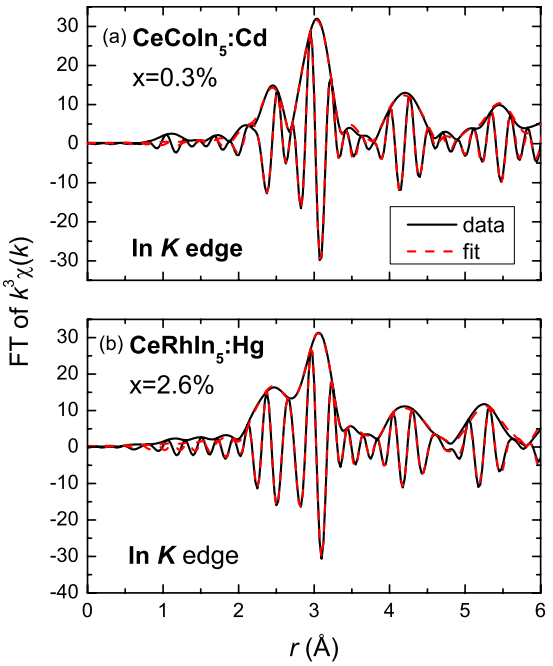

FIG. 4. (Color online) Representative fits to FT of $k^3(\chi(k)$ In K-edge data. All transforms are between 2.5–16.0 Å^{-1} after Gaussian narrowing by 0.3 Å^{-1} unless otherwise noted. The outer envelope is the modulus, and the oscillating line is the real part of the complex transform. The difference in Co and Rh backscattering is demonstrated by the large difference in the first peak near 2.5 Å, due primarily to (a) In(2)-Co or (b) In(2)-Rh scattering paths.

not explicitly reported are σ^2 parameters. However, all of these fall within reasonable limits, never exceeding about 0.006 Å^2.

Reported errors are determined using a Monte Carlo method[28] that does not properly account for systematic errors. The possible magnitude of systematic errors is discussed in Sec. III below.

III. RESULTS

Fourier transforms (FTs) of the $k^3\chi(k)$ data from the In K edge are shown in Fig. 4, which demonstrate several of the important features of the other transforms discussed in this article. The largest peak is due to several overlapping In-In and In-Ce pairs, as discussed above and indicated in Tables I–III. The peak position r is shifted from the actual pair distance R due to a phase shift of the photoelectron that occurs both as the electron leaves and returns to the absorbing atom and at the backscattering atom. This shift is well reproduced by FEFF7, allowing accurate bond lengths to be determined from the fits.[24] The real part of the transform, which is shown as the oscillating line between the modulus envelope in the FT figures, gives an indication of this phase shift as a function of the backscattering atomic species. In particular, Rh is a stronger back scatterer than Co and has a much larger phase shift. Therefore, the In-Rh peak near $r \sim 2.5$ Å is larger, but nearly out of phase with the In-Co peak. Transforms of In K-edge data at different M concentrations (not shown) change very little, indicating the small effect each substituent has on the average crystal structure.

TABLE I. Fit results for In K-edge data at 30 K on $CeRh(In_{0.991}Hg_{0.009})_5$. All scattering paths are included within the fitting range, but only those single-scattering paths with independent pair distances are reported here. All other path distances are constrained to these paths. Fit range is between 2.2 and 6.1 Å. The k^3-weighted data are transformed between 2.5–16.0 Å^{-1} after Gaussian narrowing by 0.3 Å^{-1}. These fits have about 20 degrees of freedom (Ref. 29). Reported errors in parentheses are from a Monte Carlo method and represent the random error associated with the fit. Systematic errors are discussed in the text. See text for further details. Note that the In K-edge fit results are primarily used to test the efficacy of the fitting model for determining the fraction of the absorbing atom on the In(1) site, $f_{\mathrm{In}(1)}$, which in nominally 0.2 for indium absorbers.

	R_{diff} [a] (Å)	N	σ^2 (Å^2)	R (Å)
In(1)-Ce	3.2923	0.47	0.0017(7)	3.270(4)
In(1)-In(2)	3.2775	0.94	0.0027(5)	3.23(6)
In(2)-Rh	2.7500	1.76	0.0023(3)	2.736(2)
In(2)-Ce	3.2775	1.76	0.0017[b]	3.27(1)
In(2)-In(2)	4.6142	0.87	0.001(1)	4.64(1)
ΔE_0	−5.6(6)			
S_0^2	0.94(6)			
$f_{\mathrm{In}(1)}$	0.12(3)			
$R(\%)$	6.13			

[a]From Ref. 30 for $CeRhIn_5$.
[b]Constrained to In(1)-Ce.

A fit of this structure to the In K-edge data from one of the samples is shown in Fig. 4 and the results are given in Table I for $CeRh(In_{1-x}Hg_x)_5$. The primary purpose of such fits is to demonstrate the efficacy of the fitting model, and therefore the final results are compared to the nominal crystal structure to help quantify any systematic errors. To this end, the measured pair distances are all close to those measured by diffraction, although outside the estimated errors. Considering that only 5 fit parameters describe all the bond lengths up to 5 Å, the systematic errors in the pair distances are expected to be within about 0.02 Å,[24] as observed. The σ^2 parameters are all small, as expected for a well-ordered crystal lattice. Of particular interest is the fraction of In atoms on the In(1) site, which is nominally 0.2. Within this fitting model, $f_{\mathrm{In}(1)} = 0.12(5)$. The fits to the In K-edge data from all the samples give similar results, so systematic errors in $f_{\mathrm{In}(1)}$ are expected to be better than 0.1. However, this error may be smaller when a higher fraction of a particular substituent species resides on the In(1) site, as determined for all the samples discussed below.

The Cd K-edge fit results for three of the $CeCo(In_{1-x}Cd_x)_5$ samples are summarized in Table II, and an example of the fit for $x=0.011$ is shown in Fig. 5(a). Two extra constraints were necessary on the bond lengths due to the distortion discussed below, and the maximum r in the fit range was limited to 5.1 Å in order to reduce the effect of multiple scattering on determining this distortion. The fit model describes the data very well, with $f_{\mathrm{In}(1)}=0.47(4)$ for the x

TABLE II. Fit results for Cd K data at 30 K on $CeCo(In_{1-x}Cd_x)_5$. Fit range is between 2.2 and 5.1 Å. The k^3-weighted data are transformed between 2.5–16.0 $Å^{-1}$ after Gaussian narrowing by 0.3 $Å.^{-1}$ These fits have about 13 degrees of freedom (Ref. 29). See Table I and text for further details.

		$x=0.003$			$x=0.005$			$x=0.011$		
	R_{diff}[a](Å)	N	σ^2 ($Å^2$)	R (Å)	N	σ^2 ($Å^2$)	R (Å)	N	σ^2 ($Å^2$)	R (Å)
Cd(1)-Ce	3.2618	1.63	0.0007(6)	3.253(7)	1.68	0.002(1)	3.246(6)	1.88	0.0013(6)	3.246(4)
Cd(1)-In(2)	3.2830	3.25	0.0043(7)	3.152(8)	3.35	0.006(1)	3.154(6)	3.71	0.0040(6)	3.157(3)
Cd(2)-Co	2.7187	1.19	0.0009(6)	2.738(6)	1.16	0.0022(8)	2.724(6)	1.06	0.0004(4)	2.735(3)
Cd(2)-Ce	3.2830	1.19	0.0007[b]	3.152	1.16	0.002[b]	3.154	1.06	0.0013[b]	3.157
ΔE_0		−3(1)			−3(1)			−1.9(7)		
S_0^2		0.9(1)			0.9(1)			0.9(1)		
$f_{In(1)}$		0.41(4)			0.42(4)			0.47(4)		
R(%)		13.6			13.2			9.9		

[a]From Ref. 30 for $CeCoIn_5$.
[b]Constrained to Cd(1)-Ce.

=0.011 sample. No obvious trend in $f_{In(1)}$ is observed with x, and a value of $f_{In(1)}=0.43(3)$ describes the fits to all the Cd-substituted samples. One can get a rough estimate of the number of Cd on In(2) sites by comparing the FT data in Fig. 5(a) to the In K-edge data in Fig. 4(a). These data show a reduction in the amplitude of the peak near $r\sim 2.5$ Å of ~80% compared to the same peak from the In edge, indicating $0.8\times 4/5\approx 64\%$ of the Cd sit on In(2) sites, while the remaining 36% occupy In(1) sites, in rough agreement with the fits. The most obvious difference, however, is in the amplitude of the peaks at longer pair distances. Although these can be fit by including lattice disorder via enhanced σ^2 parameters with a fit quality factor R(%) of about 18.4%, the fit quality is substantially improved by allowing for a local contraction of about 0.2 Å of the c axis near Cd atoms. The c axis in the fit in Table II is 7.32(3) Å, compared to a value of 7.5513 Å obtained by diffraction on pure $CeCoIn_5$.[30] Meanwhile, these Cd K-edge fits indicate $a=4.602(7)$ Å and $z=0.297(7)$ [position along c of In(2) plane], in reasonable agreement with the values from diffraction on $CeCoIn_5$ of $a_{diff}=4.6129$ Å and $z_{diff}=0.3094$. As a consequence of this c-axis distortion, the overlapping Cd(1)-Ce, Cd(1)-In(2), In(2)-Ce, etc., peak positions are split by ~0.1 Å, causing the dominant peak in the In edge FTs in Fig. 4(a) to be strongly suppressed in the Cd edge FTs in Fig. 5. The same argument holds for the peaks for longer pair distances.

Data and fit results to the other Cd-substituted samples are similar, in spite of the obvious, and apparently systematic, differences in the transforms shown in Fig. 6. These differences are described well by the fit parameters shown in Table

TABLE III. Fit results from Hg L_{III}-edge data on $CeT(In_{(1-x)}Hg_x)_5$. Fit range is between 2.2 and 6.1 Å. The k^3-weighted data are transformed between 2.5–16.0 $Å^{-1}$, except the T=Ir data, which are k weighted and transformed between 2.5–11.5 $Å^{-1}$. All data are Gaussian narrowed by 0.3 $Å^{-1}$ before transforming. The degrees of freedom for these fits are about 20 for the T=Co and Rh data, and about 8 for the T=Ir data (Ref. 29). See Table I and text for further details.

		T=Co, x=0.010			T=Rh, x=0.026			T=Ir, x=0.018		
	R_{diff} [a](Å)	N	σ^2 ($Å^2$)	R (Å)	N	σ^2 ($Å^2$)	R (Å)	N	σ^2 ($Å^2$)	R (Å)
Hg(1)-Ce	3.2923	2.78	0.0022(7)	3.247(2)	3.67	0.0012(8)	3.278(2)	4.00	0.003(3)	3.27(1)
Hg(1)-In(2)	3.2775	5.55	0.008(1)	3.22(2)	7.32	0.0022(8)	3.228(3)	8.00	0.005(2)	3.21(1)
Hg(2)-Co	2.7500	0.61	0.007(4)	2.76(1)	0.17	0.02(1)	2.7(1)	0.00		
Hg(2)-Ce	3.2775	0.61	0.0022[b]	3.2(1)	0.17	0.0012[b]	3.1(1)	0.00		
Hg(2)-In(2)	4.6142	0.30	0.02(1)	4.58(7)	0.08	0.040	4.8(2)	0.00		
ΔE_0		−0.3(6)			−2.4(6)			−0.9(8)		
S_0^2		0.56(7)			0.77(6)			1.0(1)		
$f_{In(1)}$		0.70(8)			0.92(4)			1.00(4)		
R(%)		9.0			12.0			27.0		

[a]From Ref. 30 for $CeRhIn_5$, repeated from Table I.
[b]Constrained to Hg(1)-Ce.

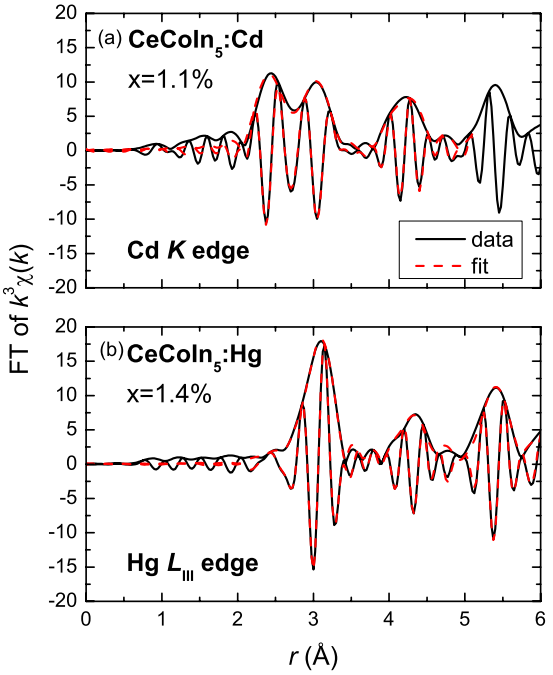

FIG. 5. (Color online) FT of $k^3(\chi(k)$ data (solid) and fit (dashed) for (a) 1.1% Cd-substituted and (b) 1.4% Hg-substituted $CeCoIn_5$. Note the large reduction in the Hg(2)-Co scattering compared to the Cd(2)-Co scattering near 2.4 Å.

II as being mostly due to differences in the mean-squared distribution widths, σ^2, for the various peaks. In particular, no trends are observed in $f_{\mathrm{In}(1)}$.

By comparison, the Hg-edge data are much more straightforward. Like both the Cd- and Sn-substituted $CeCoIn_5$ samples, Hg substitutes more strongly onto the In(1) site than would be described by a random occupancy (20%). However, Hg prefers the In(1) site even more than the other substituents, with $f_{\mathrm{In}(1)} \approx 70\%$ (see Table III). For T=Rh, Hg

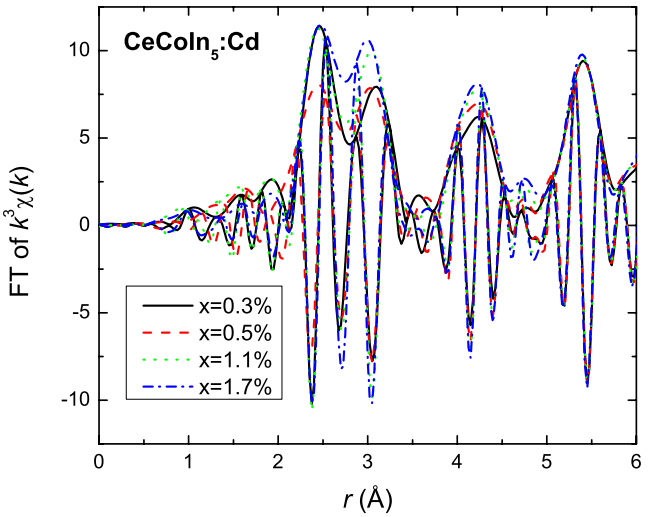

FIG. 6. (Color online) FT of $k^3(\chi(k)$ data for all measured Cd-substituted samples. Note changes in local structure. Despite these changes, no clear trends with x are deduced from the fit results.

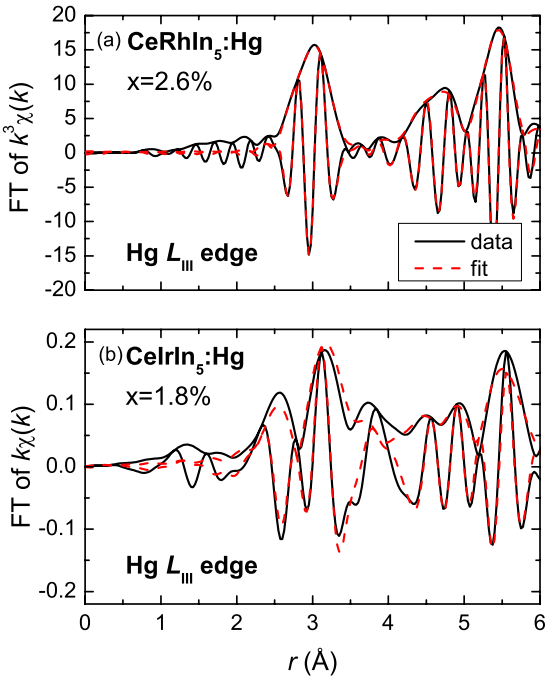

FIG. 7. (Color online) FT of $k^3(\chi(k)$ data (solid) and fit (dashed) for (a) 2.6% Hg-substituted $CeRhIn_5$ and (b) 1.8% Hg-substituted $CeIrIn_5$. Data in panel (b) are transformed between 2.5 and 11.5 $Å^{-1}$ after Gaussian narrowing by 0.3 $Å^{-1}$, in contrast to the 2.5 and 16.0 $Å^{-1}$ range used for all other data presented here. The apparent peak at 2.6 Å is actually an interference dip at ~2.8 Å as a consequence of the different transform range. No evidence for Hg(2)-Ir scattering is observed.

sits almost uniformly on the In(1) site, with little change to the local lattice. This result is clearly visible both in the data and fits shown in Figs. 5(b) and 7(a), and in the fit results in Table III. A strong correlation exists in the fits between the σ^2 parameters from the Hg(2) sites and $f_{\mathrm{In}(1)}$, whereby a large Hg(2) σ^2 reduces $f_{\mathrm{In}(1)}$. Such a correlation is expected for high $f_{\mathrm{In}(1)}$, since very little, if any, of the EXAFS signal will be coming from the Hg(2) sites, and EXAFS amplitudes vary as $1/\sigma$. Some of these Hg(2) σ^2 parameters had to be limited to 0.04 $Å^2$ in the fits to keep them from being arbitrarily large. Data and fit results on the other $CeRh(In_{1-x}Hg_x)_5$ samples are similar, with $f_{\mathrm{In}(1)}$=0.92(4).

Fit results on $CeIr(In_{1-x}Hg_x)_5$, while consistent with 100% of the Hg on In(1) sites, are of lesser quality [Fig. 7(b)] with a much larger $R(\%)$ value (Table III), possibly indicating that not all of the Hg substitutes into the $CeIrIn_5$ lattice. Reducing the emphasis on the high-k data by k-weighting the data, as opposed to k^3-weighting the data as done elsewhere in this study, improved the fit somewhat, consistent with the presence of an impurity phase. Preliminary nuclear quadrupole resonance (NQR) data also show that not all of the Hg is in a simple In-like site in the crystal lattice.[31] A strong possibility is that a small fraction of the Hg exists in another phase, probably some kind of Hg-In binary alloy, although including scattering paths from common Hg-In alloys, such as HgIn, did not improve the fit quality. It is important to recall that EXAFS selects the Hg atoms, even though they only exist in about 1% of the lattice, and so a possible 20% Hg-

phase fraction would only translate to 0.2% of the sample, yet still account for the misfit in the Hg-edge data. In any case, there remains no evidence of a Hg-Ir peak near 2.8 Å, indicating none of the Hg sits on the In(2) site.

IV. DISCUSSION

The difference in the local environment around the In(1) and In(2) sites is substantial, with a nearest-neighbor pair distance of half an angstrom shorter from the In(2) site. It is therefore not surprising that a given substituent onto the In sites would prefer the In(1) site, and, in fact, the measured distributions track the atomic radii both of the substituent species M and of the transition-metal species T. Specifically, the calculated radii for In is 2.00 Å, while for Cd, Sn, and Hg, it is 1.71, 1.72, and 1.76 Å, respectively.[32] These values track the respective occupancies $f_{\mathrm{In}(1)}$ in $CeCo(In_{1-x}M_x)_5$ of 43(3)%, 55(5)%,[12] and 71(5)%, assuming no dependence on x. The occupancies $f_{\mathrm{In}(1)}$ in $CeT(In_{1-x}Hg_x)_5$ also track how constricted the In(2) environment is by the T species: the atomic radii of Co, Rh, and Ir, are 1.67, 1.83, and 1.87 Å, respectively, a situation that is also reflected in the measured In(2)$-T$ distance in the average crystal structures of $CeTIn_5$.[30] It is worth pointing out that this situation is not unique in anisotropic crystal structures with two very different sites for a given atomic species. For instance, there are two Cu sites in $YBa_2Cu_3O_7$, and substitutions of Cu with Co are almost uniformly on the chain Cu(1) site (e.g., see Refs. 33 and 34).

Placing the impurity preferentially into the Ce-In(1) plane undoubtedly affects the progression of SC and AFM phases with M concentration, x. This point has been argued with respect to Sn substitutions, where it was found that $T_c \rightarrow 0$ K roughly when the mean separation between impurities within a plane is about equal to the superconducting coherence length in the pure material.[12] Although this may be the dominant effect in rapidly reducing T_c with respect to x, more subtle effects likely determine the variation between samples with Cd, Sn, and Hg substitutions in $CeCoIn_5$. For one, even though $f_{\mathrm{In}(1)}$ is slightly smaller for Cd substitutions compared to Sn, superconductivity is destroyed more quickly with x for Cd than Sn (Fig. 2). One can argue that this difference is due to the fundamental Ce/In charge interaction differences between these materials, since one is hole doped while the other is electron doped. In that case, one should directly compare the hole-doped, Cd- and Hg-substituted systems. The ratio between the critical concentrations, x_c, where superconductivity is destroyed between Cd (1.7%) and Hg (1.4%) is about 1.2. This value is close to the square of the ratio of $f_{\mathrm{In}(1)}$ for Hg and Cd of about 1.3, further supporting the notion of strong scattering for the in-plane In(1)-site impurities. Although this argument seems to explain differences in x_c based on $f_{\mathrm{In}(1)}$, it doesn't explain all the differences between Cd and Hg substitutions in $CeCoIn_5$. For example, T_c is higher for all $0.8<x<1.4\%$ in Hg-substituted samples compared to Cd-substituted samples, despite the much higher In(1) occupancy of Hg. These results indicate that while qualitatively the degree of In(1)-site occupancy plays a role, the detailed electronic structure around an impurity is at least as important in determining quantitative behavior and the possible role of a "local pressure" effect around the M atom.

The effect of structural disorder on the electronic and magnetic properties introduced by percent-level substitutions on the In sites remains enigmatic. The central dichotomy is between the observations of dramatic changes in the ground-state properties and the small changes in the lattice parameters. In fact, one expects less than 0.004 Å reduction in the lattice parameters at x_c based on the atomic radii. Diffraction measurements (Sec. II) on the Cd-substituted material indicate a lattice contraction consistent with this value. Measurements on the Sn- and Hg-substituted samples, however, have not been able to identify such a contraction. In any case, such a small distortion should have a relatively small effect on the magnetic coupling strength $\mathcal{J}\varrho$, where $\mathcal{J}$ is the local moment/conduction-electron exchange parameter and ϱ is the electronic density of states at the Fermi level. For instance, $\mathcal{J} \propto V_{fc}^2$, the hybridization matrix element, which goes as $1/R^5$ in a tight-binding model,[35,36] where R is the distance between the Ce and In atoms. This formula implies a less than 1% increase in V_{fc}. Countering this change, the p-electron orbital radius of all the substituents discussed here causes an overall *decrease* in V_{fc} with x relative to the pure compound. Similarly, even if each substituent changes the local density of states by 50%, the average change would be less than 1% at x_c, positive for Sn and negative for Cd and Hg. Consequently, $\mathcal{J}$ should be nearly constant for Sn and decrease by less than 2% for Cd and Hg. Because of these small changes in the average structure and conduction-electron concentrations, it is difficult to rationalize the dramatic changes in the ground state in these materials, even if one argues that the undoped system lies near a sharp band. One can argue[12] that the SC state is very sensitive to small amounts of disorder; however, such an argument can't easily apply to the sharp increase in T_N observed in the Cd- and Hg-substituted samples. In any case, there are other indications that the electronic structure is remarkably sensitive to small local structure changes. For example, dynamical mean-field theory calculations on $CeIrIn_5$ indicate that the hybridization of the Ce-In(2) bond is stronger than that of the Ce-In(1) bond despite nearly equal bond distances, giving rise to two hybridization gaps in the optical conductivity at ~30 and ~70 meV, in agreement with experiment.[37]

A clue for resolving this issue of how the In-site substituents control the physics of the $CeTIn_5$ compounds comes from recent NQR experiments on Cd-substituted $CeCoIn_5$.[38] The In NQR data taken on pure $CeCoIn_5$ (SC only), 1% (coexistent AFM and SC order), and 1.5% (only AFM) Cd-substituted samples indicate that the changes in electronic structure occur locally around a substituent atom. This conjecture is supported by NQR data in the normal state, which show that the spin-lattice relaxation rate is nearly identical despite radical changes in the ground state. It is expected that large changes in the spin-fluctuation spectrum, and hence $1/T_1$, should occur in the evolution from a SC to an AFM state, and is observed in systems such as $CeCu_2(Si,Ge)_2$.[39] However, if Cd nucleates magnetism on a scale less than the magnetic correlation length, for instance, by changing the Ruderman-Kittel-Kasuya-Yosida (RKKY) interaction

through a change in ϱ or $\mathcal{J}$, then there will be little change in $1/T_1$. Only when the substituent concentration is large enough such that the magnetic correlation lengths overlap does long-range order develop. For the sake of argument, consider only correlations in the *ab* plane and Cd atoms on the In(1). Long-range antiferromagnetic order develops at about $x=0.8\%$, or about 0.5% of the In(1) sites occupied with Cd. The mean separation between Cd atoms along the *a* or *b* directions is therefore about 14 lattice spacings. Inelastic neutron-scattering measurements on $CeCoIn_5$ reveal[40] that the dynamic correlation length in the *ab* plane is about $\xi_{ab}=9.6$ Å, which is only about two lattice spacings. The antiferromagnetic droplets would then have to increase sevenfold in this simplified two-dimensional model to overlap and generate long-range magnetic order. Nuclear magnetic resonance measurements, in fact, show indications of such an increase in ξ below 10 K in a Cd-substituted sample.[41]

The picture that is emerging is reminiscent of the Kondo disorder[42,43] and antiferromagnetic Griffiths' phase[44] discussions around compounds like UCu_4Pd and $U_{1-x}Y_xPd_3$.[45] These arguments revolve around the magnetic coupling strength $\mathcal{J}\varrho$, and the Doniach argument regarding the competing Kondo interaction and RKKY effects.[46] Here, the reduction in T_c in the electron-doped material occurs due to the distribution of scattering centers and the strong Abrikosov-Gorkov-type (AG) scattering mechanism,[17] only requiring local increases in the Kondo temperature around a scattering center.[12] In the hole-doped, Cd- and Hg-substituted systems, ϱ changes with x, apparently enough to allow RKKY interactions to dominate over the Kondo effect, potentially allowing antiferromagnetic droplets to form within a Griffiths' mechanism around impurity sites, consistent with the NQR observations.[38] Within this picture, in both the electron-doped, Kondo-disorder/AG, regime and the hole-doped, AFM Griffiths phase regime, lattice disorder plays a key role in the development of various properties with x by allowing the precipitation of larger-scale perturbations, either by disturbing the coherence of the large SC state or by precipitating long-range magnetic interactions. Although these qualitative ideas may indeed play a defining role in determining the properties in substituted 115s, a quantitative theory has not yet been developed that properly accounts for the details of this quantum critical system.

V. CONCLUSION

The fraction of *M* atoms on In(1) sites is determined in $CeT(In_{1-x}M_x)_5$ as a function of *M* in $CeCo(In_{1-x}M_x)_5$ and as a function of *T* in $CeT(In_{1-x}M_x)_5$ with *T*=Co, Rh, and Ir, using EXAFS measurements at the In *K*, Cd *K*, and Hg L_{III} edges. Fits to the In *K*-edge data indicate no measurable change in the average structure with these substituents. Fits to the Cd *K*-edge data for $CeCo(In_{1-x}Cd_x)_5$ indicate about $f_{In(1)}=43(3)\%$ of Cd atoms reside on In(1) sites, independent of x and similar to previous results[12] of $f_{In(1)}=55(5)\%$ for Sn in $CeCo(In_{1-x}Sn_x)_5$. In addition to this strong preference to occupy the In(1) site (random occupation would be $f_{In(1)}=20\%$ in this structure), the local lattice is distorted around Cd sites, consistent with a local decrease in the *c* axis of about 0.2 Å, while the *a*-lattice constant and the *z* parameter describing the position of the In(2) planes remain unchanged. These results contrast with those from the Hg L_{III}-edge data that indicate $f_{In(1)}=71(5)\%$ in $CeCo(In_{1-x}Hg_x)_5$, with only minimal changes to the local lattice structure. Moreover, $f_{In(1)}$ increases to 92(4)% for *T*=Rh and 100(10)% for *T*=Ir. While these results are rationalized in terms of the atomic radii of the *M* and *T* species and gross changes in the superconducting transition temperature, the dramatic changes in the ground state, especially in the hole-doped materials, are difficult to understand in terms of localized impurity scatterers. Rather, a sharper division can be made based on electron-versus hole-doped samples and allowing for the possibility of antiferromagnetic droplet formation. Therefore, while strong conduction-electron scattering around In(1)-site defects undoubtedly plays a large, and possibly majority, role in the progression of T_c with x, a complete understanding of the differences in the ground states requires a more thorough understanding of the actual electronic structure around defect atoms and their effect on the system as a whole.

ACKNOWLEDGMENTS

This work was supported by the U.S. Department of Energy (DOE) under Contract No. DE-AC02-05CH11231 (Lawrence Berkeley National Laboratory), by the National Science Foundation (NSF) under Grants No. DMR 0854781 (University of California, Irvine) and No. DMR-0756281 (Louisiana State University), and further supported by the U.S. DOE (Los Alamos). X-ray absorption data were collected at the Stanford Synchrotron Radiation Lightsource, a national user facility operated by Stanford University on behalf of the DOE, Office of Basic Energy Sciences.

[1] J. D. Thompson, M. Nicklas, A. Bianchi, R. Movshovich, A. Llobet, W. Bao, A. Malinowski, M. F. Hundley, N. O. Moreno, P. G. Pagliuso, J. L. Sarrao, S. Nakatsuki, Z. Fisk, R. Borth, E. Lengyel, N. Oeschler, G. Sparn, and F. Stehlich, Physica B **329-333**, 446 (2003).

[2] H. Hegger, C. Petrovic, E. G. Moshopoulou, M. F. Hundley, J. L. Sarrao, Z. Fisk, and J. D. Thompson, Phys. Rev. Lett. **84**, 4986 (2000).

[3] T. Park, F. Ronning, H. Q. Yuan, M. B. Salamon, R. Movshovich, J. L. Sarrao, and J. D. Thompson, Nature (London) **440**, 65 (2006).

[4] V. S. Zapf, E. J. Freeman, E. D. Bauer, J. Petricka, C. Sirvent, N. A. Frederick, R. P. Dickey, and M. B. Maple, Phys. Rev. B **65**, 014506 (2001).

[5] P. G. Pagliuso, C. Petrovic, R. Movshovich, D. Hall, M. F. Hundley, J. L. Sarrao, J. D. Thompson, and Z. Fisk, Phys. Rev. B **64**, 100503(R) (2001).

[6] A. Bianchi, R. Movshovich, C. Capan, P. G. Pagliuso, and J. L.

Sarrao, Phys. Rev. Lett. **91**, 187004 (2003).
[7] B.-L. Young, R. R. Urbano, N. J. Curro, J. D. Thompson, J. L. Sarrao, A. B. Vorontsov, and M. J. Graf, Phys. Rev. Lett. **98**, 036402 (2007).
[8] V. F. Mitrović, M. Horvatić, C. Berthier, G. Knebel, G. Lapertot, and J. Flouquet, Phys. Rev. Lett. **97**, 117002 (2006).
[9] E. D. Bauer, D. Mixson, F. Ronning, N. Hur, R. Movshovich, J. D. Thompson, J. L. Sarrao, M. F. Hundley, P. H. Tobash, and S. Bobev, Physica B **378-380**, 142 (2006).
[10] L. D. Pham, T. Park, S. Maquilon, J. D. Thompson, and Z. Fisk, Phys. Rev. Lett. **97**, 056404 (2006).
[11] E. D. Bauer, F. Ronning, S. Marquilon, L. D. Pham, J. D. Thompson, and Z. Fisk, Physica B **403**, 1135 (2008).
[12] M. Daniel, E. D. Bauer, S.-W. Han, C. H. Booth, A. L. Cornelius, P. G. Pagliuso, and J. L. Sarrao, Phys. Rev. Lett. **95**, 016406 (2005).
[13] M. Nicklas, O. Stockert, T. Park, K. Habicht, K. Kiefer, L. D. Pham, J. D. Thompson, Z. Fisk, and F. Steglich, Phys. Rev. B **76**, 052401 (2007).
[14] E. D. Bauer, C. Capan, F. Ronning, R. Movshovich, J. D. Thompson, and J. L. Sarrao, Phys. Rev. Lett. **94**, 047001 (2005).
[15] E. D. Bauer, F. Ronning, C. Capan, M. J. Graf, D. Vandervelde, H. Q. Yuan, M. B. Salamon, D. J. Mixson, N. O. Moreno, S. R. Brown, J. D. Thompson, R. Movshovich, M. F. Hundley, J. L. Sarrao, P. G. Pagliuso, and S. M. Kauzlarich, Phys. Rev. B **73**, 245109 (2006).
[16] C. Petrovic, S. L. Bud'ko, V. G. Kogan, and P. C. Canfield, Phys. Rev. B **66**, 054534 (2002).
[17] A. A. Abrikosov and L. P. Gor'kov, Sov. Phys. JETP **12**, 1243 (1961).
[18] E. Müller-Hartmann and J. Zittartz, Phys. Rev. Lett. **26**, 428 (1971).
[19] J. Paglione, T. A. Sayles, P.-C. Ho, J. R. Jeffries, and M. B. Maple, Nat. Phys. **3**, 703 (2007).
[20] E. D. Bauer (unpublished).
[21] T. M. Hayes and J. B. Boyce, in *Solid State Physics*, edited by H. Ehrenreich, F. Seitz, and D. Turnbull (Academic, New York, 1982), Vol. 37, p. 173.
[22] http://lise.lbl.gov/RSXAP/
[23] A. L. Ankudinov and J. J. Rehr, Phys. Rev. B **56**, R1712 (1997).
[24] G. G. Li, F. Bridges, and C. H. Booth, Phys. Rev. B **52**, 6332 (1995).
[25] J. Goulon, C. Goulon-Ginet, R. Cortes, and J. M. Dubois, J. Phys. (Paris) **43**, 539 (1982).
[26] L. Tröger, D. Arvanitis, K. Baberschke, H. Michaelis, U. Grimm, and E. Zschech, Phys. Rev. B **46**, 3283 (1992).
[27] C. H. Booth and F. Bridges, Phys. Scr. **T115**, 202 (2005).
[28] J. M. Lawrence, P. S. Riseborough, C. H. Booth, J. L. Sarrao, J. D. Thompson, and R. Osborn, Phys. Rev. B **63**, 054427 (2001).
[29] E. A. Stern, M. Qian, Y. Yacoby, S. M. Heald, and H. Maeda, Physica C **209**, 331 (1993).
[30] E. G. Moshopoulou, J. L. Sarrao, P. G. Pagliuso, N. O. Moreno, J. D. Thompson, Z. Fisk, and R. M. Ibberson, Appl. Phys. A **74**, S895 (2002).
[31] R. Urbano (private communication).
[32] E. Clementi, D. L. Raimondi, and W. P. Reinhardt, J. Chem. Phys. **47**, 1300 (1967).
[33] P. F. Miceli, J. M. Tarascon, L. H. Greene, P. Barboux, F. J. Rotella, and J. D. Jorgensen, Phys. Rev. B **37**, 5932 (1988).
[34] F. Bridges, J. B. Boyce, T. Claeson, T. H. Geballe, and J. M. Tarascon, Phys. Rev. B **39**, 11603 (1989).
[35] W. A. Harrison and G. K. Straub, Phys. Rev. B **36**, 2695 (1987).
[36] W. A. Harrison, *Elementary Electronic Structure* (World Scientific, London, 1999), p. 644.
[37] J. H. Shim, K. Haule, and G. Kotliar, Science **318**, 1615 (2007).
[38] R. R. Urbano, B.-L. Young, N. J. Curro, J. D. Thompson, L. D. Pham, and Z. Fisk, Phys. Rev. Lett. **99**, 146402 (2007).
[39] Y. Kitaoka, Y. Kawasaki, T. Miko, S. Kawasaki, G.-q. Zheng, K. Ishida, D. Aoki, Y. Haga, R. Settai, Y. Onuki, G. Geibel, and F. Steglich, J. Phys. Chem. Solids **63**, 1141 (2002).
[40] C. Stock, C. Broholm, J. Hudis, H. J. Kang, and C. Petrovic, Phys. Rev. Lett. **100**, 087001 (2008).
[41] N. J. Curro, Rep. Prog. Phys. **72**, 026502 (2009).
[42] E. Miranda, V. Dobrosavljević, and G. Kotliar, Phys. Rev. Lett. **78**, 290 (1997).
[43] E. Miranda and V. Dobrosavljević, Phys. Rev. Lett. **86**, 264 (2001).
[44] A. H. Castro Neto and B. A. Jones, Phys. Rev. B **62**, 14975 (2000).
[45] G. R. Stewart, Rev. Mod. Phys. **73**, 797 (2001).
[46] S. Doniach, Physica B **91**, 231 (1977).